Mechanical properties of the cell wall material of closed-cell Al foam

Insu Jeon[1, a], Kiyotaka Katou[2,b], Tsutomu Sonoda[2,c] and Tadashi Asahina[2,d]

[1]School of Mechanical Systems Engineering, Chonnam National University300 Yongbong-dong, Buk-gu, Gwangju, 500-757, Republic of Korea

2Full Materials Research Institute for Sustainable Development, National Institute of Advanced Industrial Science and Technology(AIST), Shimoshidami, Moriyama-ku, Nagoya, 463-8560, Japan

ai_jeon@chonnam.ac.kr, bkiyokata.katou@aist.go.jp, ctsutomu.sonoda@aist.go.jp, dt.asahina@aist.go.jp

Keywords: Closed-cell Al foam, Cell wall, Compression test, Finite element analysis, Mechanical properties

Abstract. A new approach is attempted to determine the mechanical properties, such as elastic modulus, yield stress and plastic hardening exponent of the cell wall of closed-cell Al foam. Firstly, the thickened Al alloy before foaming its molten material using blowing agent is used for fabricating tension test specimens. With the specimens, the fundamental stress-strain curve for the cell wall material is measured by means of uniaxial tension tests. Secondly, two very small and completely different structures of the Al foam are selected and used for experimental compression tests, and also directly modeled for finite element analysis based on the concept of reverse engineering. Finally, numerical analyses for the compression tests are carried out using the two modeled foam structures and various mechanical properties deviated from the fundamental curve for the cell wall material. Then, the actual mechanical properties are determined by comparing the computed stress-strain curves under compression and the measured ones. Through this research, we show a reasonable and an effective method for determining the mechanical properties of the cell wall of various cellular materials.

Introduction

As a functional light weight material, closed-cell Al foam is widely used in transportation applications, military equipment, machine tools and so on. Therefore, the mechanical performances of the foam material, including its effective elastic modulus, compressive strength, and energy absorption capacity, have become an important subject of research. Much research has been done on performance improvement of the foam material. Two main streams of research have been developed subsequently: first, the analysis of the significant effects of geometric parameters related to the cell structure on the performance of the foam material [1-7], and second, the analysis on the effects of the cell wall material properties on the performance of the foam material [8].

With respect to the effects of the geometric parameters, decreased cell size and increased thickness of the cell wall increase the compressive strength of the aluminum foam material [1,2]. Furthermore, cell face curvatures and corrugations decrease the elastic modulus and plastic collapse stress [3]. The wavy imperfection and cell shape variation decrease the stiffness of foam materials [4,5]. The effects of cell wall microstructures, which are formed differently depending on the production processes and the composition of the cell wall raw materials, on the compressive response of closed-cell foams were also presented [6]. Recently, the effects of intrinsic structural defects of the closed-cell Al foam on the decrease of the effective modulus as well as the plateau stress of the foam material have been reported [7].

With respect to the effects of the material properties of the cell wall, research results have not been extensive. Jeon et al. [8], however, demonstrated the effects of cell wall plastic properties, such as the 0.2% yield stress and power-law hardening exponent, on the energy absorption capacity of the closed-cell Al foam. They also compared the stress-strain curve measured from the a uniaxial compression test on a 10x10x10mm^3 closed-cell Al foam with the stress-strain curves obtained from

numerical simulations of the test. Although the plastic properties of the cell wall contribute significantly to the mechanical performance of the foam material, research on the measurement of the precise values of these properties have been limited.

An approximation method was applied to measure the yield stress of the Al cell wall, which takes the yield stress values to be one-third of the cell wall hardness [9-11]. Another measurement method using nanoindentation has been recently introduced to measure cell wall mechanical properties [12,13]. This method, however, has some difficulties in obtaining actual cell wall mechanical properties: it usually uses the indentation load-displacement curves, which include considerable variations arising from the inhomogeneous microstructure of the cell wall cross section, and can not account for the effect of cell wall oxidation in the measurement of the mechanical properties.

In this research, we suggest a new approach to determine the mechanical properties of the cell wall of the closed-cell Al foam. After measuring the mechanical properties of the cell wall base material, taken from a thickened Al-1.5wt%Ca alloy before foaming, we perform a direct finite element modeling (Jeon et al. [8]) of two actual 5x5x5mm^3 foam specimens. Uniaxial compression tests using the specimens and numerical simulations of the tests using the finite element models are carried out. In the simulations, the mechanical properties selected from the measured properties of the base material are used. Then, the cell wall mechanical properties and their effects on the compressive behavior of foam materials are precisely determined by comparing the computed force-displacement curves with the measured ones.

Mechanical properties of the cell wall base material

This A 6x6x12cm^3 cell wall base material ingot, taken from a thickened Al-1.5wt%Ca alloy before foaming, was prepared to measure the mechanical properties of the base material, in order to establish the limit values of the mechanical properties of the Al cell wall. From the ingot, three cylindrical specimens of 25mm height and 12.7mm diameter were fabricated by using the electrical discharge machine for the uniaxial compression test. The compression tests were carried out by using a universal testing machine AG-I of SHIMADZU Corp. with a 100kN load cell. The specimens were compressed between two circular steel compression platens of 200mm in diameter. Three strain gauges were attached on each specimen surface to measure the precise strain values (see Fig. 1). A displacement rate of 0.5mm/min was applied to the top surface of the specimen. The strain was accurately determined only up to 3.5% because of the measurement limitation of the strain gauge. The three, measured, true stress-true strain curves are shown in Fig. 2.

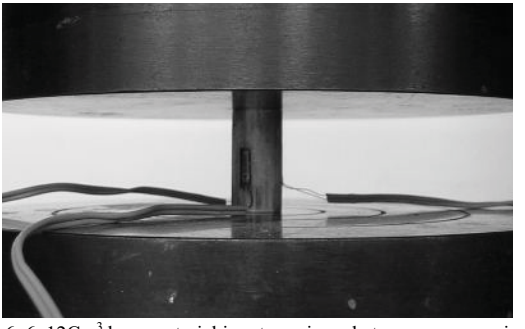

Fig. 1 A 6x6x12Cm^3 base material ingot specimen between compression platens

From the curves in Fig. 2, the elastic modulus E and elastic limit stress σ_e were obtained and tabulated together with their average values, $E = 61.7GPa$ and $\sigma_e = 11.16MPa$. The nonlinear part of the curves can be fitted by using the Ramberg–Osgood model as follows:

$$\frac{\bar{\varepsilon}^p}{\varepsilon_e} = \alpha\left(\frac{\bar{\sigma}}{\sigma_e}\right)^n \quad \text{for } \bar{\sigma} > \sigma_e \tag{1}$$

where $\bar{\sigma}$, the Mises stress; $\bar{\varepsilon}^p$, the equivalent plastic strain; $\varepsilon_e = \sigma_e / E$, the reference strain component; α, a non-dimensional constant set to "1" for computation; n, the power-law hardening exponent.

The properly fitted curve using the Ramberg-Osgood model for the measured curves of the base material is plotted together in Fig. 2. For this curve fitting, the power-law hardening exponent, n, was determined as 3 obtained from the comparison of the measured curves with the calculated curves after substituting $E = 61.7GPa$ and $\sigma_e = 11.16MPa$, and various n values into Eqn. (1).

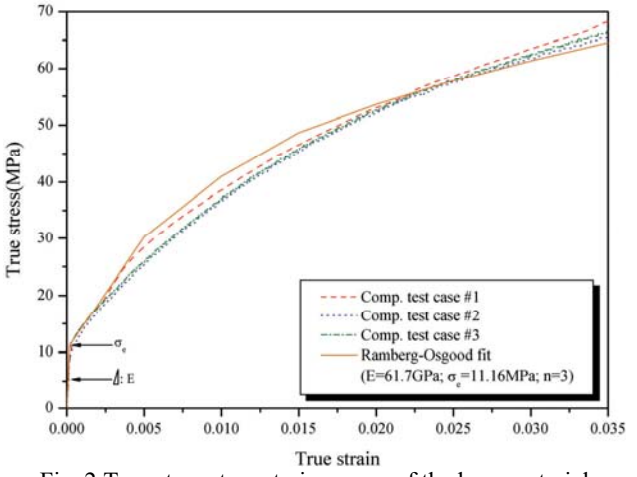

Fig. 2 True stress-true strain curves of the base material

Finite element modeling of the two foam specimens

A thorough introduction of the direct finite element modeling procedure for a closed-cell foam was presented [8]. Following the procedure, two 5x5x5mm^3 foam specimens A and B were modeled independently. The microfocus X-ray CT system of Shimadzu Corp. was used to scan the outer and inner structures of the specimens. The scanned grayscale tomographic images of the specimens A and B are obtained. Using these images, each foam specimen was reconstructed using a 3D reconstruction program TRI/3D-BON of Ratoc System Engineering Co. Ltd. The profile of the cellular structure and the air region of a specimen in the tomographic images were binarized using the 3D reconstruction program and the isolated small particles from the cellular structure in the binarized images were removed. The 3D cellular structures were then reconstructed using the marching cubes algorithm (see Figs. 3(c) and 4(c)) [8,14].

For geometric modeling of each foam specimen, every cell in each reconstructed model was disjointed, and all the disjointed cells were modified and smoothened one by one to fabricate their nonuniform rationale B-spline (NURBS) surfaces. For simplicity of modeling, all inner voids having maximum diameters that were less than 0.1mm were disregarded. Then, the NURBS surfaces were fabricated using each cell. Two geometric solids for the two foam specimens were constructed using Boolean operations between two 5x5x5mm^3 geometric solid cubes and the outer and inner NURBS surfaces of each specimen. The 3D scanned data processing software RapidForm^{TM} of INUS Tech. Inc. was used for all geometric modeling [8,15].

Subsequently, compatible 3D finite element meshes were generated directly in each fabricated geometric solid after iterative calculations using the commercial mesh generation software PATRAN of MSC Software Corp. In this process the volume errors, $\frac{V_m - V_a}{V_a}$, where V_m is the volume of the meshed model and V_a is the actual volume of the specimen, were 5.5% for Specimen A and 4.94% for Specimen B, respectively.

Using the finite element models, two Al foam specimens between two platens were completely modeled. Quadratic tetrahedral elements with 10 nodes were used for the specimens and platens. The total number of elements and nodes used for specimen A were 79311 and 145725, and for specimen B were 75994 and 137585, respectively. For simulating the compression test process, a package code ABAQUS of Dassault Systems was used. The incremental plasticity theory of isotropic-hardening materials was selected for the elastic-plastic behavior of the specimens, which uses the objective stress rate for finite deformation of the Al cell wall. Moreover, the power-law hardening rule in Eqn. (1) was used to calculate the plastic hardening index in the incremental plasticity theory [8,16-18] for the simulations, x- and y-direction degrees of freedom were constrained at several nodes around the center on the lower surface of each specimen to prevent rigid body motions, and z-direction displacement was loaded at over 20% strain on the top surface of each upper platen. The frictionless contact condition was applied to the contact surfaces between the specimens and the platens.

As for the material properties of the platens, $E = 214GPa$ and $\nu = 0.3$ of Tool Steel SKS3 were applied. For the Al cell wall, various values of the power-law hardening exponents, n=3, 5, 6, 8.5, 9 and elastic limit stresses, σ_e=11.16, 25, 28, 30, 31, 32, 34MPa, were selected; these various values were the measured mechanical properties of the cell wall base material and selected values based on the measured values. For the cell wall elastic modulus, E=61.7GPa of the base material, E=68GPa of the published values of ALPORAS [9] and E=73.1GPa of Aluminum 2024-T6 were selected for the numerical tests.

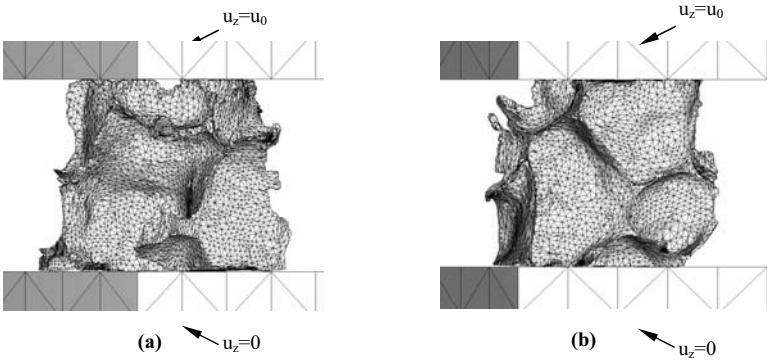

Fig. 3 (a) Finite element models of Specimen A and (b) Specimen B between two platens

Uniaxial compression tests of the two foam specimens

A universal testing machine AG-I of SHIMADZU Corp. with a *5kN* load cell was used for the uniaxial compression tests of the two 5x5x5mm^3 foam specimens. The specimens were compressed between two circular platens of *100mm* in diameter, which was sufficiently larger than the specimens (see Figs. 3(a) and 3(b)). A displacement rate of 0.15mm/min was applied to the top surface of the specimens up to *60%* strain to obtain the entire compressive behavior of the foam specimens. Because of the difficulty in attaching the strain gauge to the nonuniform surfaces of the foam specimens, the machine compliance, which represents the relation between the displacement of the testing machine and the applied loading, was used to determine precise specimen displacements [7].

Results and discussion

The force-displacement curves of the specimens A and B obtained from the experimental measurements and the numerical simulations are plotted in Figs. 4(a) and 4(b), respectively. To define the changes in the obtained force-displacement curves, three evaluation parameters were introduced: the peak force in the curves, f_{peak}, the displacement at the peak force, δ_{peak}, and the elastic stiffness in the elastic interval of the curves, f/δ.

The computed force-displacement curves of each specimen using the same values of $n = 8.5$ and $\sigma_e = 31MPa$, and three different elastic moduli, E =61.7, 68, and 73.1GPa are shown compared with the measured curves in Figs. 4(a) and 4(b). In these figures, it is hard to find significant differences among the computed curves. This means that the effect of the elastic moduli of the cell wall in the range of a general Al alloy, E =61.7-73.1GPa, on the force-displacement curve is very small. Table 1 shows the % errors of the evaluation parameters obtained from the curves. In Table 1, all of the % error values stay within 10% and close to the volumetric errors of the specimens. Therefore, we selected the elastic modulus of the Al cell wall to be E =68GPa, which was also measured by Sugimura et al. [9].

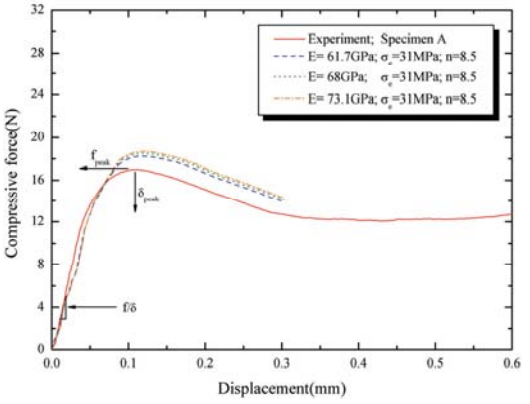

(a)

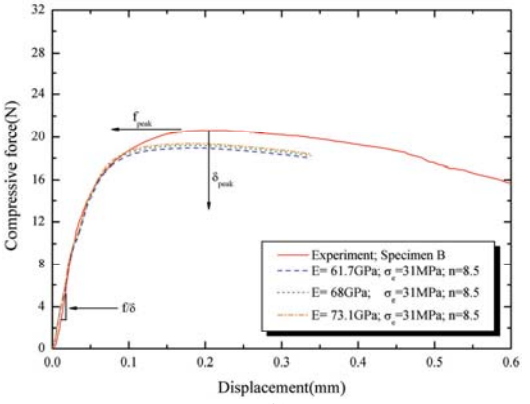

(b)

Fig. 4 Effects of the elastic modulus on the force-displacement curve of (a) Specimen A and (b) Specimen B

Table 1 % errors of the evaluation parameters according to the changes in the elastic modulus, E

	E (GPa)	σ_e (MPa)	n	δ_{peak} error(%)		f_{peak} error(%)		Stiffness(f/δ) error(%)	
				Spec. A	Spec. B	Spec. A	Spec. B	Spec. A	Spec. B
Cal. #1	61.7	31	8.5	-5.24655	8.78983	-7.08129	8.14667	5.40935	7.87728
Cal. #2	68*	31	8.5	-8.86144	8.70942	-8.51777	7.01161	1.19502	8.66801
Cal. #3	73.1	31	8.5	-9.86208	9.05619	-9.57739	6.14852	-0.2301	6.65899

(*see Sugimura et al. [9])

References

[1] T. Miyoshi, M. Itoh, S. Akiyama and A. Kitahara: Adv. Eng. Mater. Vol. 2 (2000), p. 179

[2] T. Miyoshi, M. Itoh, T. Mukai, H. Kanahashi, H. Kohzu, S. Tanabe and K. Higashi: Scripta Mater. Vol. 41 (1999), p. 1055

[3] A.E. Simone and L.J. Gibson: Acta Mater. Vol. 46 (1998), p. 3929

[4] J.L. Grenestedt: J. Mech. Phys. Solids Vol. 46 (1998), p. 29

[5] J.L. Grenestedt and K. Tanaka: Scripta Mater. Vol. 40 (1999), p. 71

[6] A.E. Markaki and T.W. Clyne: Acta Mater. Vol. 49 (2001), p. 1677

[7] I. Jeon and T. Asahina: Acta Mater. Vol. 53 (2005), p. 3415

[8] I. Jeon, T. Asahina K.J. Kang and S. Im: submitted to Int. J. Plasticity (2008)

[9] Y. Sugimura, J. Meyer, M.Y. He, H. Bart-Smith, J. Grenstedt and A.G. Evans: Acta Mater. Vol. 45 (1997), p. 5245

[10] A.E. Simone and L.J. Gibson: Acta Mater. Vol. 46 (1998), p. 3109

[11] E. Andrews, W. Sanders and L.J. Gibson: Mater. Sci. Eng. A Vol. 270 (1999), p. 113

[12] A. Kim and K. Tunvir: J. Mech. Sci. Technol. Vol. 20 (2006), p. 819

[13] M.A. Hasan, A. Kim and H.J. Lee: Compos. Struct. Vol. 83 (2008), p. 180

[14] T. Sone, T. Tamada, Y. Jo, H. Miyoshi and M. Fukunaga: Bone Vol. 35 (2004), p. 432

[15] D.S. Shin, K. Lee and D. Kim: Comput.-Aided Des. Vol. 39 (2007), p. 559

[16] R.M. McMeeking: J. Mech. Phys. Solids Vol. 25 (1977), p. 357

[17] I. Jeon and S. Im: J. Mech. Phys. Solids Vol. 49 (2001), p. 2789

[18] Y.H. Lee, B.K. Lee, I. Jeon and K.J. Kang: Acta Mater. Vol. 55 (2007), p. 6084